Journal of Solid State Chemistry 183 (2010) 242–249

Contents lists available at ScienceDirect

Journal of Solid State Chemistry

journal homepage: www.elsevier.com/locate/jssc

First principles calculations of electronic structure and magnetic properties of Cr-based magnetic semiconductors $Al_{1-x}Cr_xX$ (X=N, P, As, Sb)

Y. Saeed [a], A. Shaukat [a], S. Nazir [b], N. Ikram [b], Ali Hussain Reshak [c,*]

[a] Department of Physics, GC University, Faisalabad 38000, Pakistan
[b] Centre for Solid State Physics, University of the Punjab, Quaid-e-Azam Campus, Lahore 54590, Pakistan
[c] Institute of Physical Biology, South Bohemia University, Nove Hrady 37333, Czech Republic

ARTICLE INFO

Article history:
Received 25 May 2009
Received in revised form
15 October 2009
Accepted 25 October 2009
Available online 11 November 2009

Keywords:
Ab-initio calculation
Dilute magnetic semiconductor
Magnetic moment
Hybridization

ABSTRACT

First principles calculations based on the density functional theory (DFT) within the local spin density approximation are performed to investigate the electronic structure and magnetic properties of Cr-based zinc blende diluted magnetic semiconductors $Al_{1-x}Cr_xX$ (X=N, P, As, Sb) for $0 \le x \le 0.50$.The behaviour of magnetic moment of $Al_{1-x}Cr_xX$ at each Cr site as well as the change in the band gap value due to spin down electrons has been studied by increasing the concentration of Cr atom and through changing X from N to Sb. Furthermore, the role of p–d hybridization is analyzed in the electronic band structure and exchange splitting of d-dominated bands. The interaction strength is stronger in $Al_{1-x}Cr_xN$ and becomes weaker in $Al_{1-x}Cr_xSb$. The band gap due to the spin down electrons decreases with the increased concentration of Cr in $Al_{1-x}Cr_xX$, and as one moves down along the isoelectronic series in the group V from N to Sb. Our calculations also verify the half-metallic ferromagnetic character in Cr doped AlX.

1. Introduction

Dilute magnetic III–V and II–VI semiconductors (DMS) doped with small amount ($<10\%$) of transition metals (TM) are being extensively studied due to their application in devices based on both magnetic and semiconductor properties. TM-doped III–V semiconductors are widely used in high speed electronic, optoelectronic and spintronics devices [1,2]. Many experiments have been performed successfully in order to search DMS materials of ferromagnetic behaviour at room temperature by doping transition metal elements in wide band gap semiconductor such as Mn-doped in InAs, GaAs, while using a variety of experimental techniques Cr-doped AlN thin films have been synthesized and are found to exhibit ferromagnetic properties at room temperature [3–8].

In Mn-based DMS, the static Jahn–Teller effect is negligible, whereas in Cr-based DMS, Cr^{2+} ions give rise to static Jahn–Teller effect—a magnetic property based on how many electrons are available to fill the energy states. Moreover, excited states of Cr^{2+} ions contribute to the magnetic properties and lead to a pronounced anisotropy of the Cr^{2+} ion energy level structure. In this regard, one of the systems that have received special attention in recent years involves Cr-doped AlN, (Al, Cr) N, whose structural, electronic and magnetic properties have recently been studied by Endo et al. [9]. Cr-doped AlN and its alloys are favourable DMS candidates because of their enhanced thermal stability, the possibility of the band-gap-engineered structures and graded barrier layers for spin-tunnelling devices [10]. Yang et al. [8] have studied Cr-doped AlN system experimentally and reported ferromagnetism at temperature over 340 K in Cr-doped AlN thin film grown by reactive co-sputtering on silicon, glass, and Kapton substrates, while Wang et al. [11] predicted short-range ferromagnetic coupling in WZ-phase $Al_{1-x}Cr_xN$ thin film using density functional calculations. Moreover, $Al_{0.93}Cr_{0.07}N_1$ alloy system has been studied experimentally and theoretically both in zinc blende (ZB) and wurtzite (WZ) phase by Wu et al. [6].

In this paper, we study the electronic structure and magnetic properties of Cr-doped AlX (X=N, P, As, Sb) with Cr concentration upto 50% in zinc blende phase by carrying out self-consistent, first principles, spin-polarized calculations based on full potential (linearized) augmented plane wave plus local orbital method (FP-LAPW+lo) within density functional theory (DFT) [12] with local spin density approximation (LSDA) for exchange and correlation [13]. Our main objective is to see the effect of Cr ions doped on the electronic structure and magnetic properties of $Al^{III}X^{V}$ compounds.

2. Computational details

As mentioned earlier, the electronic and magnetic properties of $Al_{1-x}Cr_xX$ (X=N, P, As, Sb) are calculated using the FP-LAPW+lo

* Corresponding author. Fax: +420 386 361231.
E-mail addresses: yasir_saeed54321@yahoo.com (Y. Saeed), schaukat@gmail.com (A. Shaukat), nazirsafdar@gmail.com (S. Nazir), nazmaikram@hotmail.com (N. Ikram), maalidph@yahoo.co.uk (A. Hussain Reshak).

0022-4596/$ - see front matter © 2009 Elsevier Inc. All rights reserved.
doi:10.1016/j.jssc.2009.10.018

method within the framework of the density functional theory (DFT) as implemented in the WIEN2 K code [14] applying LSDA for exchange-correlation potential. The non-overlapping muffin-tin radii R_{MT} of Al, N, P, As, Sb and Cr are taken to be as large as possible. Within the muffin-tin spheres, the *l*-expansion of the non-spherical potential is carried out up to l_{max}=10 while the charge density is Fourier expanded up to G_{max}=24. In order to achieve energy eigenvalues convergence, the wave functions in the interstitial region are expanded in terms of plane waves with a cut-off of $K_{MAX}=8/R_{MT}$. A mesh of 72 special **k**-points are taken in the irreducible wedge of the Brillouin zone (IBZ).

The bulk Al*X* (*X*=N, P, As, Sb) has zinc blende structure with space group $F\bar{4}3m$ in which the Al atom is located at (0, 0, 0) and X atom at (0.25, 0.25, 0.25). When Cr is doped with concentration *x* =0.25, the calculations are formed with an eight-atom supercell, constructed by taking $1\times1\times1$ standard unit cell of structure with cubic symmetry belong to space group $P\bar{4}3m$. In eight-atom supercell, we replace one Al atom at (0, 0, 0) by Cr and keep the other three Al atoms and four *X* atoms ($Al_3Cr_1X_4$) at their position.

For *x*=0.5, we replace two Al atoms and get a tetragonal structure with space group $P\bar{4}m2$. We construct the $1\times1\times2$ supercell with 16 atoms for *x*=0.125 structure with space group $P\bar{4}2m$. We replace the first atom by Cr and so obtained ratio of Cr in this structure is $Al_7Cr_1X_8$. All these structures reflect the fact that each Al (or Cr) atom has four anions (*X*) as the nearest neighbours and each anion (*X*) has four cations (Cr and Al) as the nearest neighbours.

3. Results and discussion

3.1. Structural properties

Before calculating the electronic structure and magnetic properties, volume optimization of $Al_{1-x}Cr_xX$ has been performed. The values of lattice constant '*a*', bulk modulus *B*, determined by fitting the total energy as a function of volume using the Murnaghan's equation of state at zero pressure [15]. The quantities '*a*', *B* and first order pressure derivative of the bulk modulus, *B*′, for different concentrations of Cr (0.0, 0.125, 0.25, 0.5) in Al*X*, and the bond lengths of Cr–Al and Cr–*X*, i.e. L_{CrAl} (Å) and L_{CrX} (Å) are displayed in Table 1. The equilibrium lattice constant 'a' as function of concentration *x* for different compounds can be described approximately by the following equations:

$$a\,(\text{Å}) = 4.4016 - 0.155x - 0.007x^2 (Al_{1-x}Cr_xN)$$

$$a\,(\text{Å}) = 5.432 - 0.096x - 0.0829x^2 (Al_{1-x}Cr_xP)$$

$$a\,(\text{Å}) = 5.631 - 0.0724x - 0.0917x^2 (Al_{1-x}Cr_xAs)$$

$$a\,(\text{Å}) = 6.1094 - 0.1347x - 0.029x^2 (Al_{1-x}Cr_xSb)$$

We find that the bulk modulus increases with the concentration *x* in all structures of (Al, Cr) *X*, as presented in Table 1.

3.2. Electronic properties

In this section, we examine the electronic structure of compounds and discuss the origin of the half-metallicity. The host valence bands in $Al^{III}X^{V}$ compounds are formed due to the anion *p* states, i.e. N 2*p*, P 3*p*, As 4*p* and Sb 5*p* in AlN, AlP, AlAs and AlSb, respectively, and show a gradual shift from lower (AlN) to the higher (AlSb) in energy values. The most important features of the electronic calculations can be seen from spin-dependent total and partial density of state (DOS) projected in Cr, Al and X muffin-tin in case of $Al_{1-x}Cr_xX$.

Table 1
The calculated equilibrium constant constants *a* (Å), bulk modulus *B* (GPa), *B*′ (GPa), length of Cr-Al bonds L_{AX} (Å) and length of Cr–*X* bonds L_{CX} (Å) for $Al_{1-x}Cr_xX$ and $Ga_{1-x}Cr_xX$ (*X*=N, P, As, Sb).

Compound	*X*	*a* (Å)	*B* (GPa)	*B*′ (GPa)	L_{AlX} (Å)	L_{CrX} (Å)
$Al_{1-x}Cr_xN$	0.00	4.404	192.33	4.05	1.9734	–
	0.125	4.376	211.55	4.11	1.8965	1.8965
	0.25	4.368	210.97	4.15	1.8812	1.8812
	0.50	4.325	209.66	4.28	1.8749	1.8749
$Al_{1-x}Cr_xP$	0.00	5.434	85.5	3.90	2.3531	–
	0.125	5.419	88.62	4.10	2.3465	2.3465
	0.25	5.404	89.40	4.25	2.340	2.340
	0.50	5.364	89.80	3.55	2.3225	2.3225
$Al_{1-x}Cr_xAs$	0.00	5.6297	74.73	4.28	2.4274	–
	0.125	5.626	74.78	4.31	2.4348	2.4348
	0.25	5.604	74.82	4.46	2.3958	2.3958
	0.50	5.573	78.73	4.33	2.3731	2.3731
$Al_{1-x}Cr_xSb$	0.00	6.109	57.15	4.45	2.6453	–
	0.125	6.094	57.23	4.87	2.6452	2.6452
	0.25	6.075	57.79	5.12	2.6306	2.6306
	0.50	6.043	58.09	5.08	2.6166	2.6166

When the transition metal (TM) atom is substituted at the cationic site, the tetrahedral crystal field formed by *X* ions splits its 3*d* states into threefold degenerate t_{2g} and double degenerate e_g levels with the T_d group symmetry for a TM atom tetrahedrally bound to *X* (*X*=N, P, As, Sb) atoms. This shows that the Cr impurity doped in $Al_{1-x}Cr_xX$ has a $4s^2\ 3d^3$ valence-electron configuration and the majority-spin Cr 3*d* states are $\frac{4}{5}$ filled, and the minority-spin Cr 3*d* states are unoccupied, while three Bohr magnetons of magnetic moment in $Al_{1-x}Cr_xX$ per Cr atom have arisen.

The total and partial DOS show the exact position of e_g and t_{2g} levels of the Cr in $Al_{1-x}Cr_xX$. We note that the t_{2g} state lies above the e_g state confirming that Cr is sitting in the tetrahedral environment in all compounds of $Al_{1-x}Cr_xX$. For the octahedral environment e_g state lies above the t_{2g} state as one would expect from the crystal field splitting. We have shown here only prototype of DOS's and band structure diagrams for $Al_{1-x}Cr_xX$ for *x*=0.125, 0.25, and 0.5 (Fig. 1).

3.2.1. $Al_{1-x}Cr_xN$

The valence band of AlSb is originated from anion 5*p* states, i.e., Sb 5*p* states, and when Al is replaced by Cr, it polarizes the host band. The partial DOS of the Cr atoms shows that the spin up Cr 3*d* bands are almost occupied while the spin down bands lie above the E_F, which gives rise to huge magnetic moments of 3 μ_B. In $Al_{0.75}Cr_{0.25}N$, we define the majority-spin that contains the largest number of electrons. In Fig. 2, the states in the energy range from −8.3 to −3.4 eV come mainly from N 2*p* states with minor contribution from Cr 3*d* and Al 3*s*, 3*p* states. The contribution of Cr 3*d* states in band structure in the majority-spin can be divided into two parts: first, the band originating from the Cr 3*d* e_g-doubly degenerate state orbitals, centred at −1 eV, and secondly the t_{2g} triply degenerate band, centred at −0.23–1.09 eV. The t_{2g} states strongly hybridize with the N 2*p* states in the case of majority-spin band.

In minority-spin 3*d* states lie closer to the bottom of conduction band and are centred at 1.2 eV due to e_g states and at 2.1 eV due to t_{2g} states. The N 2*p* and 3*d* states form the top of the valence band at around −3.53 eV. The 3*d* states lie above the N 2*p* states, so that their mutual repulsion simultaneously drives

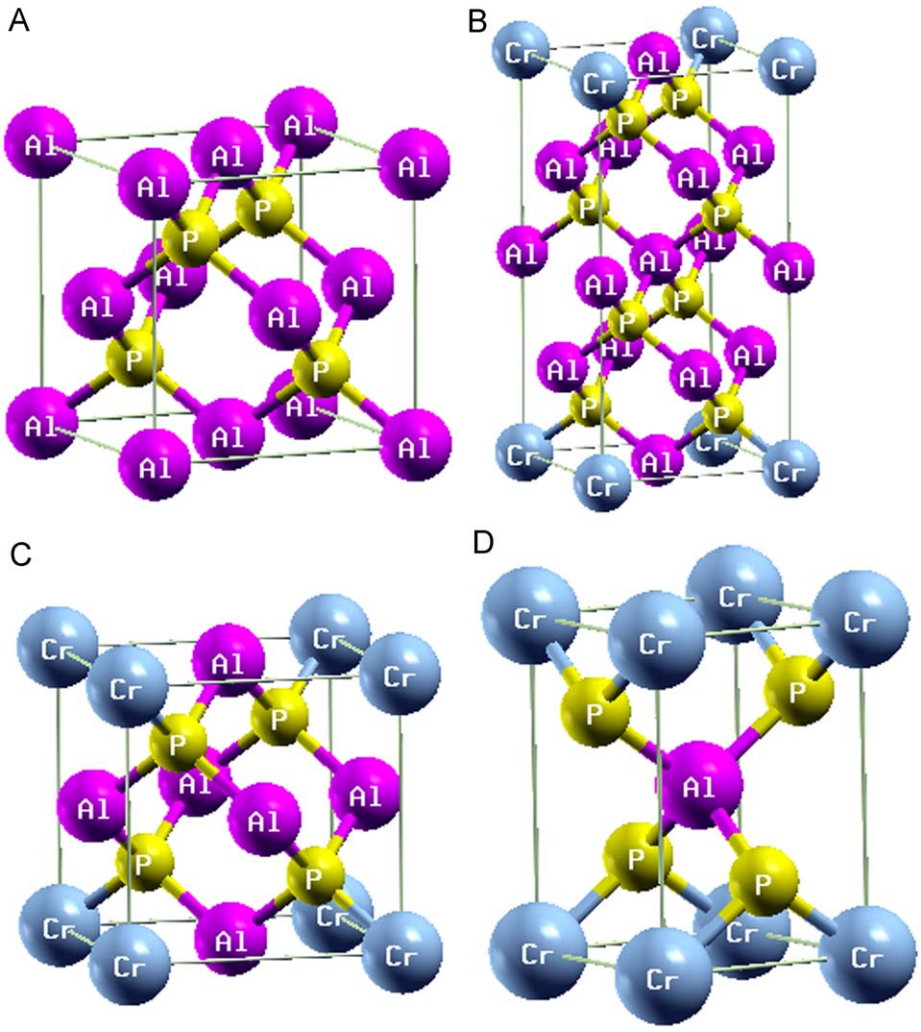

Fig. 1. The prototype structures of Cr doped AlX (X=N, P, As, Sb) compounds: (A) zinc blende AlP for x=0, (B) $Cr_1Al_7P_8$ for x=0.125, (C) $Cr_1Al_3P_4$ for x=0.25, and (D) $Cr_1Al_1P_4$ for x=0.5.

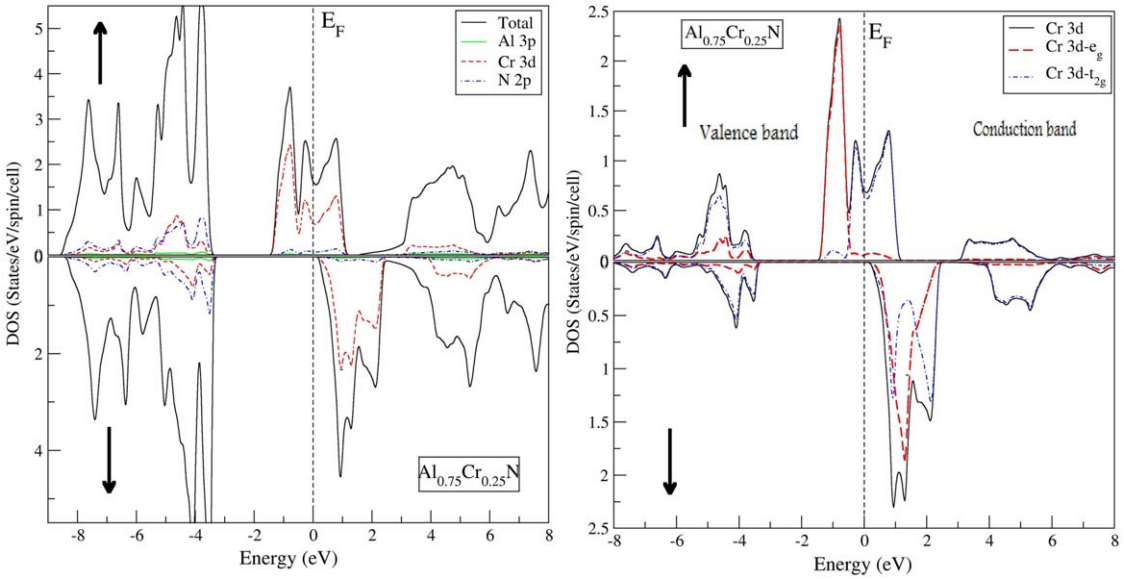

Fig. 2. Total and partial DOS projected on to the Cr impurity site, for majority-spin and minority-spin for $Al_{0.75}Cr_{0.25}N$.

the 3*d* band up above the Fermi level and *p* band down below the Fermi level, thereby giving rise to the metallic conduction band. When the Fermi level is running through the impurity band, the $Al_{1-x}Cr_xN$ alloys are half metallic. Due to large *p*–*d* exchange interaction, there is a narrow band gap formed in majority-spin electrons, the band gap is much wider with values of 3.45, 3.4 and 3.3 eV for $Al_{0.875}Cr_{0.125}N$, $Al_{0.75}Cr_{0.25}N$ and $Al_{0.50}Cr_{0.50}N$, respectively, as shown in Fig. 3. It is noted that the band gap decreases with increased the concentration of Cr in AlN.

3.2.2. $Al_{1-x}Cr_xP$

The total and partial densities of states as well as the band structure of $Al_{0.75}Cr_{0.25}P$ are shown in Figs. 4 and 5, respectively. The majority-spin electrons form the top of the valence band from −4 to −0.3 eV. It is dominated by P 3*p* and 3*d*–e_g states which are completely filled, but 3*d*-t_{2g} partially filled states, which lie in midst of the Fermi level, cause the metallic nature of the ternary alloy. On the other hand, for the minority-spin, the valence band from −6.29 to −1.32 eV is formed due to the Al 3*p* and P 3*p* states and the bottom of the conduction band from 0.21 to 1.92 eV are dominated by the e_g and t_{2g} states. We see that the hybridization of t_{2g} with P 3*p* states at around −2.6 and −2.8 eV in $Al_{0.75}Cr_{0.25}P$ and $Al_{0.50}Cr_{0.50}P$, respectively.

With concentration of Cr up to 50% in $Al_{1-x}Cr_xP$, the bands formed due to the majority-spin electrons are metallic in nature and energy band due to the minority-spin electrons has band gap of 1.65, 1.6, and 1.6 eV for x=0.125, 0.25 and 0.50 $Al_{1-x}Cr_xN$, respectively, as shown in Fig. 5.

3.2.3. $Al_{1-x}Cr_xAs$

Fig. 6 shows the spin-dependent total and partial densities of states for DOS of $Al_{0.75}Cr_{0.25}As$. For majority-spin, from −6 to

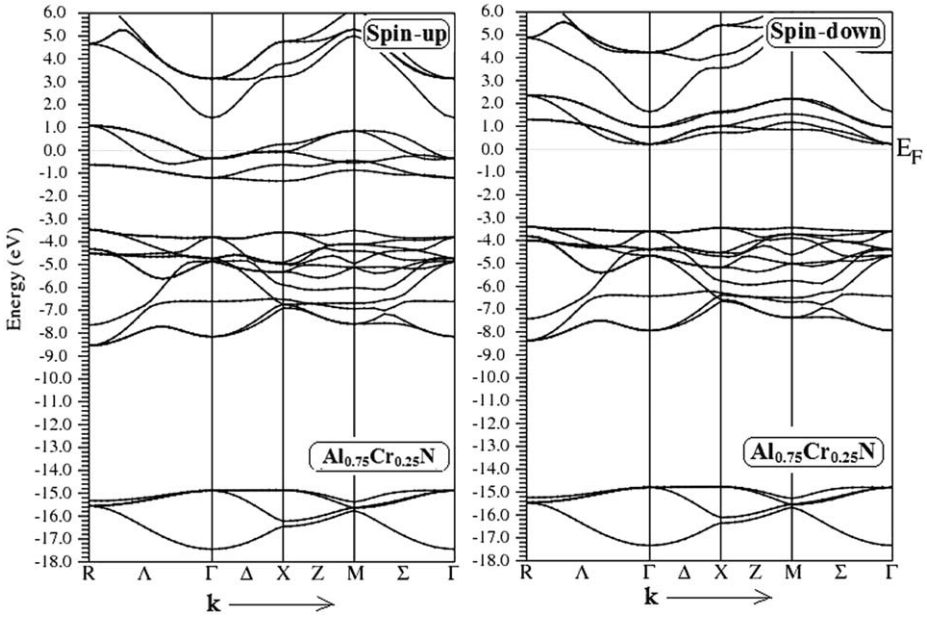

Fig. 3. Spin-polarized band structures for majority-spin and minority-spin for $Al_{0.75}Cr_{0.25}N$.

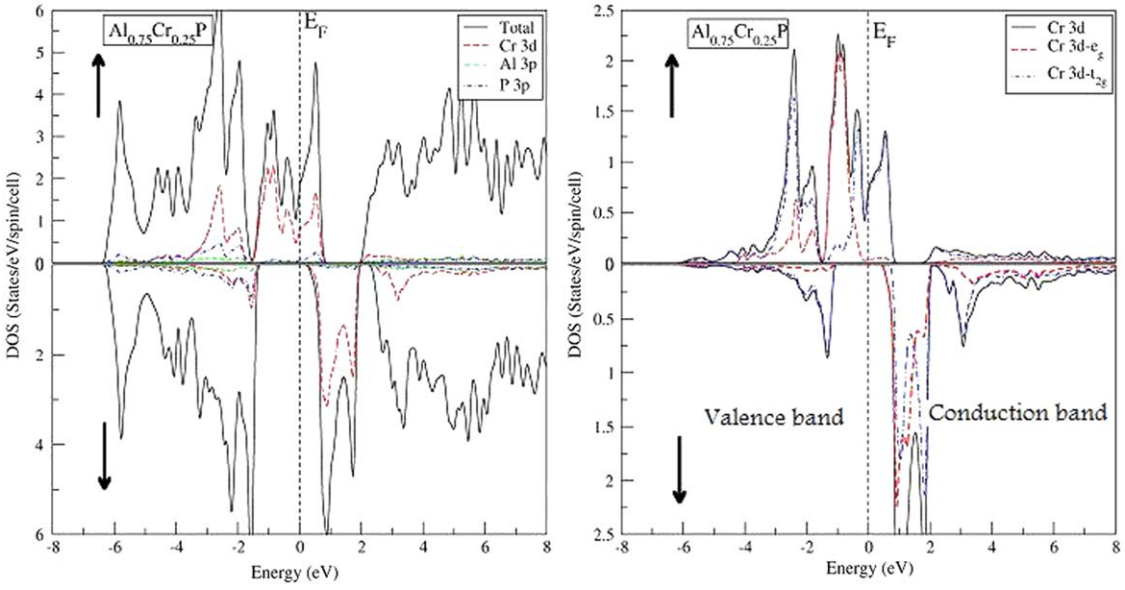

Fig. 4. Total and Partial DOS projected on to the Cr impurity site, for majority-spin and minority-spin for $Al_{0.75}Cr_{0.25}P$.

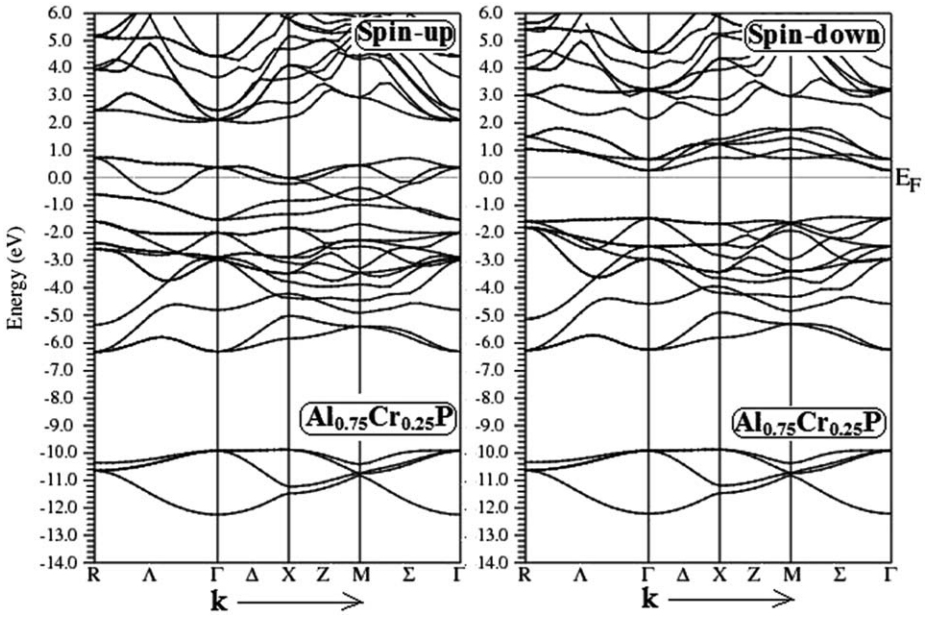

Fig. 5. Spin-polarized band structures for majority-spin and minority-spin for $Al_{0.75}Cr_{0.25}N$.

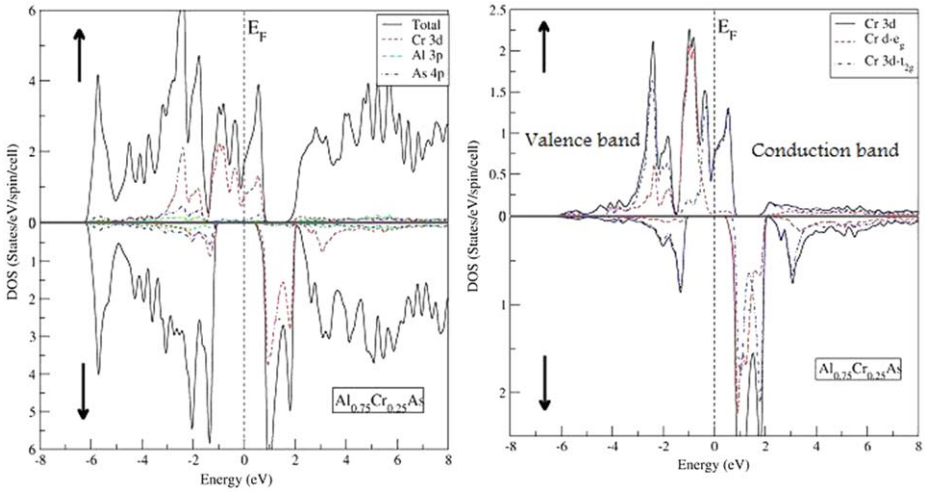

Fig. 6. Total and partial DOS projected on to the Cr impurity site, for majority-spin and minority-spin for $Al_{0.75}Cr_{0.25}As$.

−4.5 eV the corresponding bands originate essentially from the Al 3*p* states, which exhibit narrow bands with a weak contribution from As 4*s* and Cr 3*p* states, while from −6.2 to −1 eV the bands are dominated by the N 2*p* and 3*d* states with a weak contribution from Al 3*p* and Cr 5*p* states.

For minority-spin, top of the valence band extends from –6.5 to –1.129 eV dominated by the As 4*p* states. We observe that the bottom of the conduction band from 0.5 to 2.0 eV is originated only due to 3*d*–e_g and t_{2g} states of Cr. For majority and minority spins, the valence band maximum (VBM) shows a large contribution from the As 4*p* states, which hybridize with the Cr 3*d* states. The band gap due to the spin down electrons has gap values of 1.6, 1.5, and 1.6 eV for x=0.125, 0.25 and 0.50 in $Al_{1-x}Cr_xAs$, respectively, as shown in Fig. 7.

3.2.4. $Al_{1-x}Cr_xSb$

In Fig. 8 we display the spin-dependent total and partial DOS for $Al_{0.75}Cr_{0.25}Sb$, where the Sb 5*p* states are seen at −2 eV for the case of majority-spin electrons. The next band is formed by the e_g orbitals at around −1 eV for majority spin and at 1.3 eV for the minority-spin. Moreover, the wider antibonding *p*–*d* t_{2g} hybridization appears to start from –2 eV for majority-spin and from –0.8 eV for minority-spin. We find considerable amplitude of Cr 3*d* component around the Fermi level and get a small DOS peak of 3*d* states at the top of the valence band.

There is a large exchange between the majority-spin and minority-spin DOS around the Fermi level. The majority-spin electrons show metallic behaviour, while there is an energy gap (spin down gap) in the band of minority-spin electrons. For the gap formed inbetween partially filled e_g states of 3*d*, the position of the gap is different for the majority and minority electrons. The band gap due to the spin down electrons is 1.15, 1.1 and 1.0 eV for x=0.125, 0.25 and 0.50 in $Al_{1-x}Cr_xSb$, respectively, as shown in Fig. 9.

The partial filling of the majority-spin state t_{2g} suggests a ferromagnetic ground state associated with the double exchange mechanism. With increasing concentration of Cr, the partially filled t_{2g} state is broadened (Fig. 10), which stabilizes the ferromagnetism in all $Al_{1-x}Cr_xX$ as reported by Zhang et al. [16]

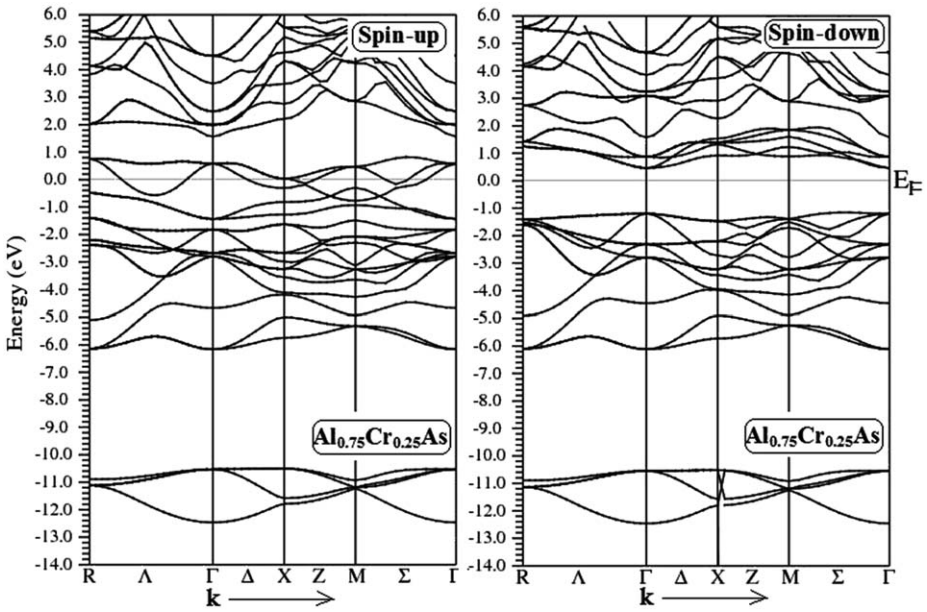

Fig. 7. Spin-polarized band structures for majority-spin and minority-spin for $Al_{0.75}Cr_{0.25}As$.

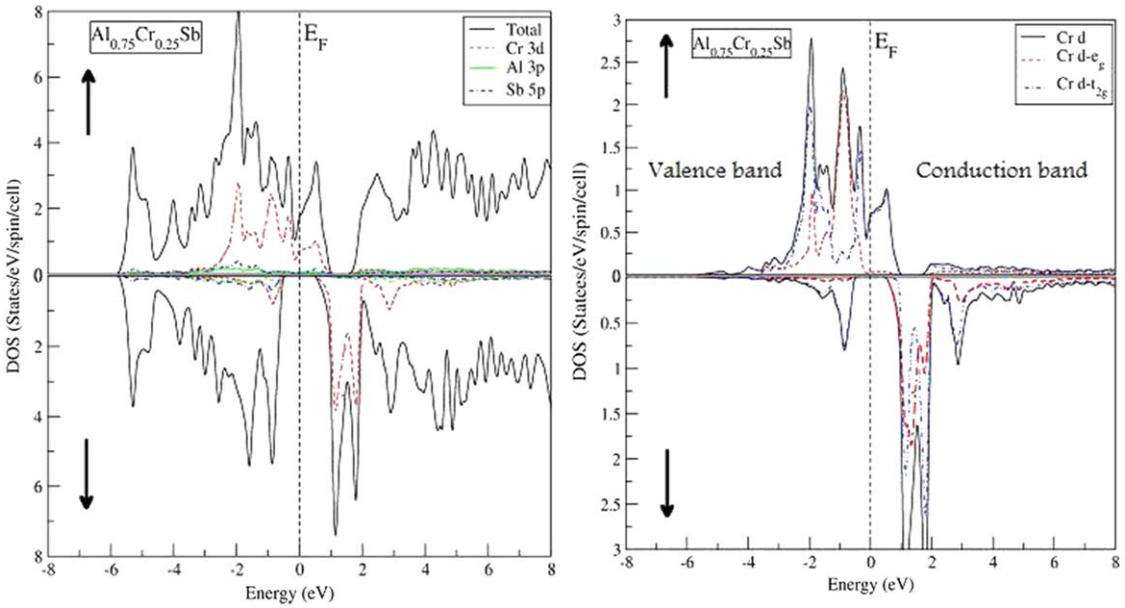

Fig. 8. Total and partial DOS projected on to the Cr impurity site, for majority-spin and minority-spin for $Al_{0.75}Cr_{0.25}Sb$.

in Cr-doped AlP calculations. The hybridization of t_{2g} and X p states around −3.8 eV for $Al_{0.75}Cr_{0.25}N$, −2.6 eV for $Al_{0.75}Cr_{0.25}P$, −2.3 eV for $Al_{0.75}Cr_{0.25}As$ and −1.8 eV for $Al_{0.75}Cr_{0.25}Sb$ can be seen in figures showing PDOS of these alloys, This shows that the hybridization of t_{2g} and X p states shift towards the Fermi level as we move down the isoelectronic series from N to Sb elements. The hybridization is stronger in $Al_{0.75}Cr_{0.25}N$ but becomes weaker in $Al_{0.75}Cr_{0.25}Sb$; it means that, in going from $Al_{1-x}Cr_xN$ to $Al_{1-x}Cr_xSb$, the interaction strength reduces particularly for the nearest neighbour interactions. Similar trend has also been observed in moving from AlMnN to AlMnSb [17]. The origin of ferromagnetism and the role of Zener's p–d exchange interaction based on model proposed by Dietl et al. [18] and that of double exchange mechanism in Mn-doped GaP and GaAS were explained by Sato et al. [19], whereas for Cr-doped AlP, this study was later undertaken by Zhang et al. [16]. These studies arrive at the same conclusion that both p–d exchange interaction and double exchange mechanism contribute to the ferromagnetism and to the stability of the ferromagnetic state. We find that the present study of $Al_{1-x}Cr_xX$ compounds also lead to similar results.

4. Magnetic properties

We have also calculated the total magnetic moments of $Al_{1-x}Cr_xX$, the local moments of Al, Cr and X and the interstitial moment. The total magnetic moment has a value of about 3.0 μ_B for all $Al_{1-x}Cr_xX$ alloys, which agrees well with the experimental

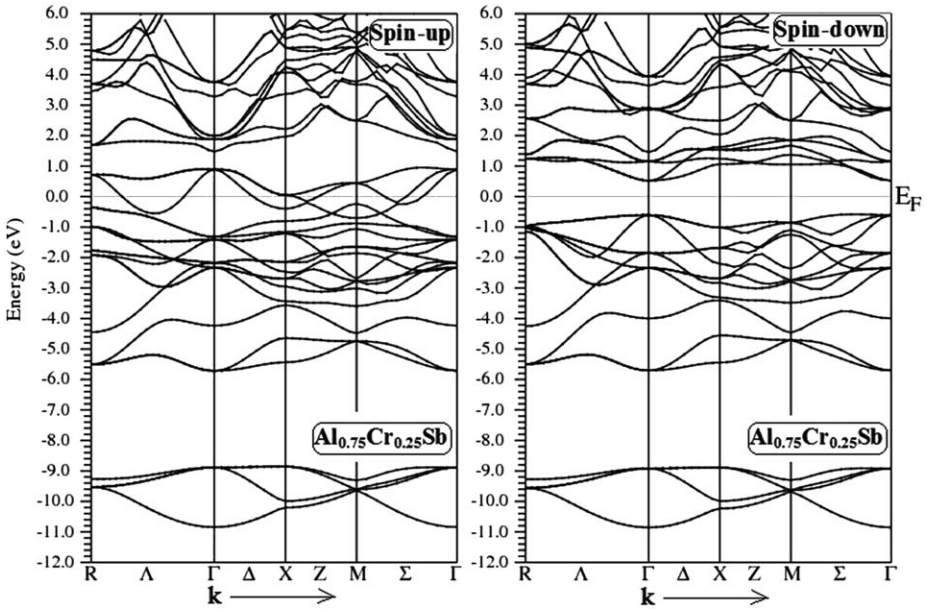

Fig. 9. Spin-polarized band structures for majority-spin and minority-spin for $Al_{0.75}Cr_{0.25}Sb$.

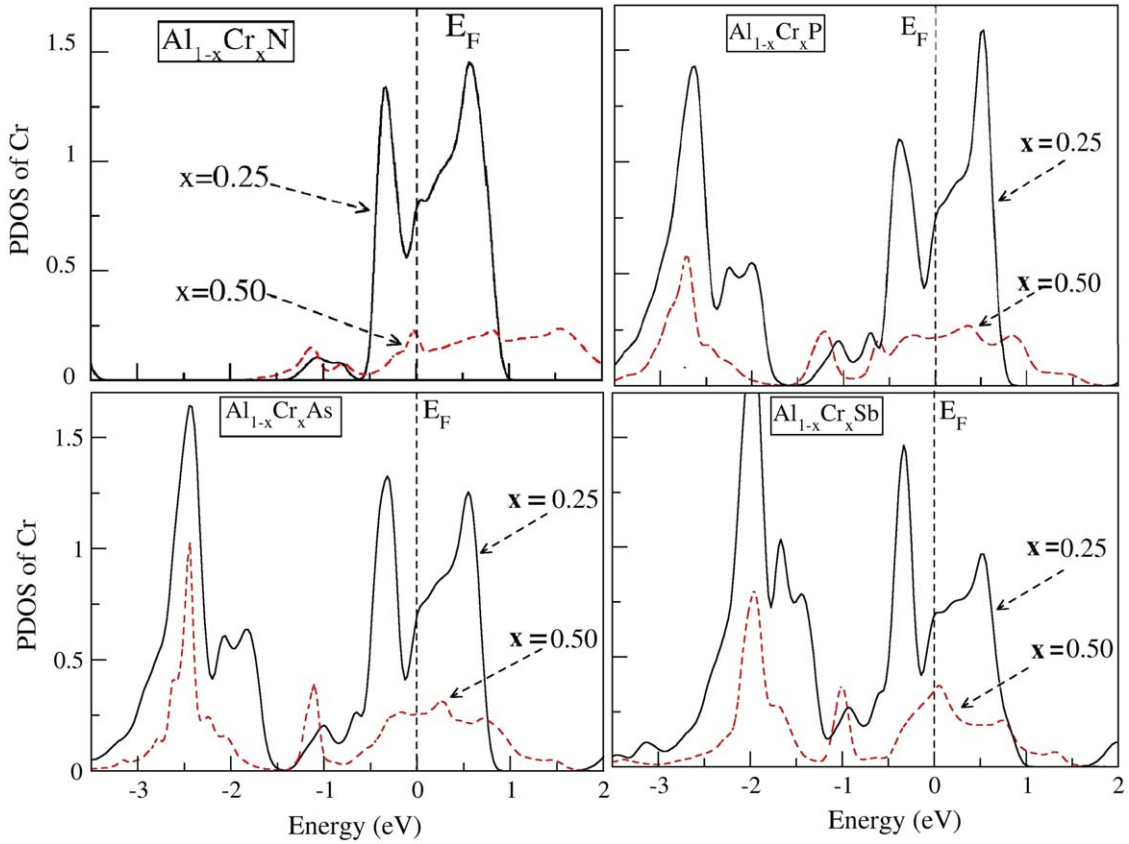

Fig. 10. Partial DOS of Cr 3*d* t_{2g} states with different concentrations of *x* for $Al_{1-x}Cr_xX$ (*x*=0.25, 0.50).

[8,20] and other theoretical [21] results on $Al_{1-x}Cr_xX$. The main part of the magnetic moment due to Cr atom is 2.2061, 2.700, 2.887 and 2.921 μ_B (μ_B is the Bohr magnetron) for $Al_{0.75}Cr_{0.25}N$, $Al_{0.75}Cr_{0.25}P$, $Al_{0.75}Cr_{0.25}As$ and $Al_{0.75}Cr_{0.25}Sb$, respectively.

We note that there is strong hybridization between $3d$–t_{2g} and *X p* states, which can yield ferromagnetic coupling between the Cr moments. This *p*–*d* hybridization reduces the local magnetic moment of Cr from its free space value ~3.0–2.2061, 2.700, 2.887, 2.921 μ_B in (Al, Cr) *X* at *x*=0.25, respectively. Our results show that the main contribution of magnetic moments is strongly localized on the Cr site (Table 2). The additional contribution to the total magnetic moment appears to come from Al and *X* atoms. As we move down the V^b column of the periodic table from $Al_{1-x}Cr_xN$ to $Al_{1-x}Cr_xSb$, the magnetic moment of Cr increases.

Table 2
Total and local magnetic moment in $Al_{1-x}Cr_xX$ (X=N, P, As, Sb) with the concentration of Cr.

Compound	X $0 \le x \le 0.5$	M^{Tot} (μ_B/cell)	m^{Cr}	m^{Al}	m^X	$m^{interstital}$
$Al_{1-x}Cr_xN$	0.00	–	–	–	–	–
	0.125	3.0	2.1672	0.0119	0.0067	0.6853
	0.25	3.0	2.2061	0.0235	0.0135	0.9781
	0.50	3.0	2.3761	0.0405	0.0335	0.9833
$Al_{1-x}Cr_x$	0.00	–	–	–	–	–
	0.125	3.0	2.6766	0.03008	−0.0026	0.03885
	0.25	3.0	2.7163	0.02983	−0.0044	0.36792
	0.50	3.0	2.7011	0.05539	−0.0623	0.3688
$Al_{1-x}Cr_xAs$	0.0	–	–	–	–	–
	0.125	3.0	2.851	0.0250	−0.0065	0.27181
	0.25	3.0	2.8580	0.0248	−0.0547	0.2582
	0.50	3.0	2.8672	0.0440	−0.0863	0.2614
$Al_{1-x}Cr_xSb$	0.00	–	–	–	–	–
	0.125	3.0	2.9143	0.0124	−0.0127	0.01172
	0.25	3.0	2.9210	0.0129	−0.0664	0.11317
	0.50	3.0	2.9496	0.0605	−0.0417	0.12632

5. Conclusion

In this work, systematic theoretical study of the electronic, magnetic and structural properties of Cr-doped $Al_{1-x}Cr_xX$ (X=N, P, As, Sb) ternary compounds with $0 \le x \le 0.50$ concentration has been undertaken, For this purpose an accurate full potential density functional method has been used. We find that the total magnetization of the cell is of the order of 3.0 μ_B per Cr atom and it remains consistent even with the change in the concentration x or anion X. The half-metallic ferromagnetism is observed in the $Al_{1-x}Cr_xN$ ternary compounds at their optimized cell volumes. The Fermi level slightly moves upward and the energy gap of the minority-spin band at the Fermi energy reduces as we go from N to Sb, and as a result, the half-metallic gaps become narrower. Furthermore, both p–d exchange interaction and double-exchange mechanism seem to be responsible for ferromagnetism.

Acknowledgements

For the author A.H. Reshak the work was supported from the institutional research concept of the Institute of Physical Biology, UFB (No. MSM6007665808).

References

[1] A.H. MacDonald, P. Spiffier, N. Samarth, Nat. Mater. 4 (2005) 195.
[2] S.A. Wolf, D.D. Awschalom, R.A. Buhrman, J.M. Daughton, S. von Molnar, M.L. Roukes, A.Y. Chtchelkanova, D.M. Treger, Science 294 (2001) 1488; I. Žutić, J. Fabian, S.D. Sarma, Rev. Mod. Phys. 76 (2004) 323.
[3] H. Munekata, H. Ohno, S. von Molnar, A. Segmuller, L.L. Chang, L. Esaki, Phys. Rev. Lett. 63 (1989) 1849.
[4] H. Ohno, A. Shen, F. Matsukura, A. Oiwa, A. Endo, S. Katsumoto, Y. Iye, Appl. Phys. Lett. 69 (1996) 363.
[5] D. Kumar, J. Antifakos, M.G. Blamire, Z.H. Barber, Appl. Phys. Lett. 84 (2004) 5004.
[6] S.Y. Wu, H.X. Liu, L. Gu, R.K. Singh, L. Budd, M. van Schilfgaarde, M.R. McCartney, D.J. Smith, N. Newman, Appl. Phys. Lett. 82 (2003) 3047.
[7] R.M. Fraizer, J. Stapleton, G.T. Thaler, C.R. Abernathy, S.J. Pearton, R. Rairigh, J. Kelly, A.F.J. Hebard, Appl. Phys. 94 (2003) 1592.
[8] S.G. Yang, A.B. Pakhomov, S.T. Hung, C.Y. Wong, Appl. Phys. Lett. 81 (2002) 2418.
[9] Y. Endo, T. Sato, A. Takita, Y. Kawamura, M. Yamamoto, IEEE. Trans. Magn. 41 (2005) 2718.
[10] G. Lin, S.Y. Wu, H.X. Liu, R.K. Singh, N. Newman, D.J.J. Simth, Magn. Magn. Mater. 290 (2005) 1395.
[11] Q. Wang, A.K. Kandalam, Q. Sun, P. Jena, Phys. Rev. B 73 (2006) 115411.
[12] P. Hohenberg, W. Kohn, Phys. Rev. B 136 (1964) 864.
[13] J.P. Perdew, Y. Wang, Phys. Rev. B 45 (1992) 13244.
[14] P. Blaha, K. Schwarz, G.K.H. Madsen, D. Kvanicka, J. Luitz, WIEN2 K, An Augmented Plane Wave+Local Orbital Program for Calculating Crystal Properties, Karlheinz Schwarz, Techn. Universitat, Wien, Austria, 2001, ISBN: 3-9501031-1-1-2.
[15] F.D. Muranghan, Proc. Natl. Acad. Sci. (USA) 30 (1944) 244.
[16] Y. Zhang, W. Liu, H. Niu, Solid State Commun. 145 (2008) 590.
[17] K. Sato, P.H. Dederichs, H.-K. Yoshida, J. Phys. Soc. Jpn. 76 (2007) 024717.
[18] T. Dietl, H. Ohno, F. Matsukura, J. Cibert, D. Ferrand, Science 287 (2000) 1019; T. Dietl, Semicond. Sci. Technol. 17 (2002) 377.
[19] K. Sato, P.H. Dederichs, H.K. Katayama-Yoshida, J. Kudmovsky, J. Phys. Condens. Matter 16 (2004) S5491.
[20] H.X. Liu, S.Y. Wu, R.K. Singh, L. Gu, D.J. Smith, N. Newman, N.R. Dilley, L. Montes, M.B. Simmonds, Appl. Phys. Lett. 85 (2004) 4076.
[21] C. Hong, Z. Jun-Feng, Y. Hong-Kuan, Commun. Theor. Phys (Beijing, China) 48 (2007) 749.